International Journal of Greenhouse Gas Control 5 (2011) 1329–1338

Contents lists available at ScienceDirect

International Journal of Greenhouse Gas Control

journal homepage: www.elsevier.com/locate/ijggc

A natural analogue for CO_2 mineral sequestration in Miocene basalt in the Kuanhsi-Chutung area, Northwestern Taiwan

Hsueh-Yu Lu[a,*], Cheng-Kuo Lin[b], Wayne Lin[b], Tai-Sheng Liou[a], Wen-Fu Chen[c], Ping-Yu Chang[d]

[a] Department of Earth and Environmental Sciences, National Chung Cheng University, 168, University Rd., Min-Hsiung, Chia-Yi, Taiwan
[b] Green Energy and Environment Research Laboratories, Industrial Technology Research Institute, Hsinchu, Taiwan
[c] Department of Tourism Management, Chia Nan University of Pharmacy and Science, Tainan, Taiwan
[d] Institute of Applied Geosciences, National Taiwan Ocean University, Taipei, Taiwan

ARTICLE INFO

Article history:
Received 17 October 2010
Received in revised form 28 May 2011
Accepted 28 May 2011
Available online 28 June 2011

Keywords:
CO_2 mineral sequestration
Mineral carbonation
Basalt
Ultramafic xenoliths

ABSTRACT

In general, CO_2 sequestration by carbonation is estimated by laboratory experimentation and geochemical simulation. In this study, however, estimation is based on a natural analogue study of the Miocene basalt in the Kuanhsi-Chutung area, Northwestern Taiwan. This region has great potential in terms of geological and geochemical environments for CO_2 sequestration. Outcropping Miocene basalt in the study area shows extensive serpentinization and carbonation. The carbon stable isotopes of carbonates lie on the depleted side of the Lohmann meteoric calcite line, which demonstrates that the carbonates most probably precipitate directly from meteoric fluid, and water–rock interaction is less involved in the carbonation process. Oxygen stable isotope examinations also show much depleted ratios, representative of product formation under low temperatures (~50–90 °C). This translates to a depth of 1–2 km, which is a practical depth for a CO_2 sequestration reservoir. According to petrographic observation and electron microprobe analysis, the diopside grains in the basalt are resistant to serpentinization and carbonation; therefore, the fluid causing alteration is likely enriched with calcium and there must be additional sources of calcium for carbon mineralization. These derived geochemical properties of the fluid support the late Miocene sandstone and enclosed basalts as having high potential for being a CO_2 sequestration reservoir. Moreover, the existing geochemical environments allow for mineralogical assemblages of ultramafic xenoliths, indicating that forsterite, orthopyroxene and feldspar minerals are readily replaced by carbonates. Based on the mineral transformation in xenoliths, the capacity of CO_2 mineral sequestration of the Miocene basalt is semi-quantitatively estimated at 94.15 kg CO_2 chemically trapped per 1 m^3 basalt. With this value, total CO_2 sequestration capacity can be evaluated by a geophysical survey of the amount of viable Miocene basalt at the potential sites. Such a survey is required in the near future.
© 2011 Elsevier Ltd. All rights reserved.

1. Introduction

Burning of fossil fuels has considerably increased the total load of CO_2 in the atmosphere. Although the long-term consequences of increasing atmospheric CO_2 are still being debated, one possible outcome is global warming as additional CO_2 and other greenhouse gases trap heat from escaping the earth's surface. This has lead to atmospheric CO_2 reduction efforts. The Intergovernmental Panel on Climate Change (IPCC) held a workshop in November 2002 in Regina, Canada to identify geological sequestration as one of several options that have the potential to help lessen the effects and costs of climate change (IPCC, 2002). The CO_2 is captured after combustion and injected back into geological reservoirs where it is immobilized by natural processes. Some potential reservoirs have been evaluated, including deep saline aquifers, depleted oil and gas fields, coal-bearing formations, and the deep ocean (IPCC, 2002). An IPCC Special Report published in 2005 made an extensive technical review on carbon dioxide capture and storage (IPCC, 2005). Underground geological storage is still one of the most effective strategies to sequestrate CO_2. Based on these guidelines, the Taiwan Government initiated the national wide Taiwan CO_2 Reduction Project (TCRP) in 2007 to develop technologies for CO_2 capture, reuse, and storage in Taiwan. This study is part of TCRP's research efforts to investigate potential geological storage sites in Taiwan.

In the IPCC Special Report on carbon dioxide capture and storage, the storage mechanisms for geological formations are categorized into structural/stratigraphic, hydrodynamic, and geochemical trappings (IPCC, 2005). Structural and stratigraphic traps are reservoir-trap-seal systems such as those that trap hydrocarbons. In the case of hydrodynamic trapping, the residence time of CO_2 in deep saline aquifers of low permeability is potentially thousands to millions of years. The CO_2 migrates through a deep saline

* Corresponding author. Tel.: +886 5 2720411x66211; fax: +886 5 2720807.
E-mail addresses: seishei@eq.ccu.edu.tw, sheilu@ccu.edu.tw (H.-Y. Lu).

1750-5836/$ – see front matter © 2011 Elsevier Ltd. All rights reserved.
doi:10.1016/j.ijggc.2011.05.037

aquifer as a separate phase on the top of the formation until it is trapped in pore spaces with poor connectivity or in local structural or stratigraphic traps. In the longer term, CO_2 will dissolve into the formation brine (Bachu et al., 1994; Allen et al., 2005). Geochemical trapping is another CO_2 storage mechanism. This mechanism has the potential to provide increased storage capacity, effectiveness, and security in terms of permanent CO_2 sequestration. The injected CO_2 can geochemically interact with pore fluid and reservoir rocks transforming it into minerals. The potential storage reservoirs include: coal beds, basalt, and ultramafic/serpentine formations, etc., all of which are beneficial to trapping CO_2 by mineralization and/or chemical absorption (e.g. Viete and Ranjith, 2007; Giammar et al., 2005). In recent years, many geochemical CO_2 sequestration projects have been conducted in large igneous provinces (LIPs), especially flood basalt and deep mafic/ultramafic rocks (e.g. McGrail et al., 2006; Schaef et al., 2010). An example of such a project is the CarbFix project established by Iceland, France and the United States. This project is focused on developing practical and cost-effective technology for carbon mineralization in basalts with the intention that CO_2 produced by the Hellisheidi geothermal power plant in Iceland will be injected into basaltic rocks in the very near future (Matter et al., 2009; Gislason et al., 2010). Moreover, India and the United States have also initiated a pilot study aimed at sequestrating CO_2 in the Deccan flood basalt of western India (Prasad et al., 2009; Goel et al., 2009). The existence of these projects demonstrates the serious consideration given to geochemical sequestration of CO_2 in mafic and ultramafic rocks and the promise such a technology has to sequestrate CO_2 for millions of years.

Because developing geochemical systems for mineral trapping are complicated, they are generally examined through laboratory experiments and geochemical modeling. Experimental studies explore mineral trapping pathways for reactions between CO_2 and pore fluids and reservoir rocks at elevated pressures and temperatures (e.g. Golubev et al., 2005; Kaszuba et al., 2003); however, under such conditions, time scales for laboratory experiments are limited, ranging from days to months. Gunter et al. (1997) were able to extend the time scale using geochemical modeling. Simulation of CO_2 sequestrations is theoretically based on thermodynamic calculations. Presently, there are three commonly used computer programs that are capable of simulating CO_2 mineral trapping, EQ3/6 (e.g. Gianelli and Grassi, 2001; Cipolli et al., 2003), GWB (e.g. Allen et al., 2005; Zerai et al., 2006) and PHREEQC (e.g. Soong et al., 2004; Wigand et al., 2008; Gysi and Stefánsson, 2008). However, when modeling the migration of CO_2 in the storage system, geochemical calculations must be coupled with multi-phase fluid flow models and the TOUGHREACT program can provide this function (Xu et al., 2004; Audigane et al., 2007).

Another method for evaluating potential and reaction pathways in mineral trapping at injection sites is the study of natural analogues. Flaathen et al. (2009) reported that dissolved inorganic carbon in groundwater decreases with basalt dissolution, which causes carbonate precipitation. In this study, similar research was conducted in the Kuanhsi-Chutung area, Taiwan. It is one of the candidate sites for Taiwan's CO_2 Reduction Project. The target reservoir formation outcrops over this area. The location is an extraordinary natural analogue for understanding the geochemical processes that occur after CO_2 injection.

2. Study area

2.1. Geological background

The Kuanhsi-Chutung area is located in Northwestern Taiwan (Fig. 1), which is part of the passive Eurasian Plate Margin. After the end of the Cretaceous period, the margin was under an extensional tectonic regime. According to stratigraphic studies of northern Taiwan (e.g. Lin and Watts, 2002), there were three depositional cycles during Miocene times (Table 1) (Tu and Chen, 1991). Each cycle records a regressive event with coastal to terrestrial deposits and a subsequent marine transgression event with offshore to nearshore deposits. The regressive sequences are dominantly composed of coal-bearing and coarse-grained sediments. These formations have the potential to store a remarkable amount

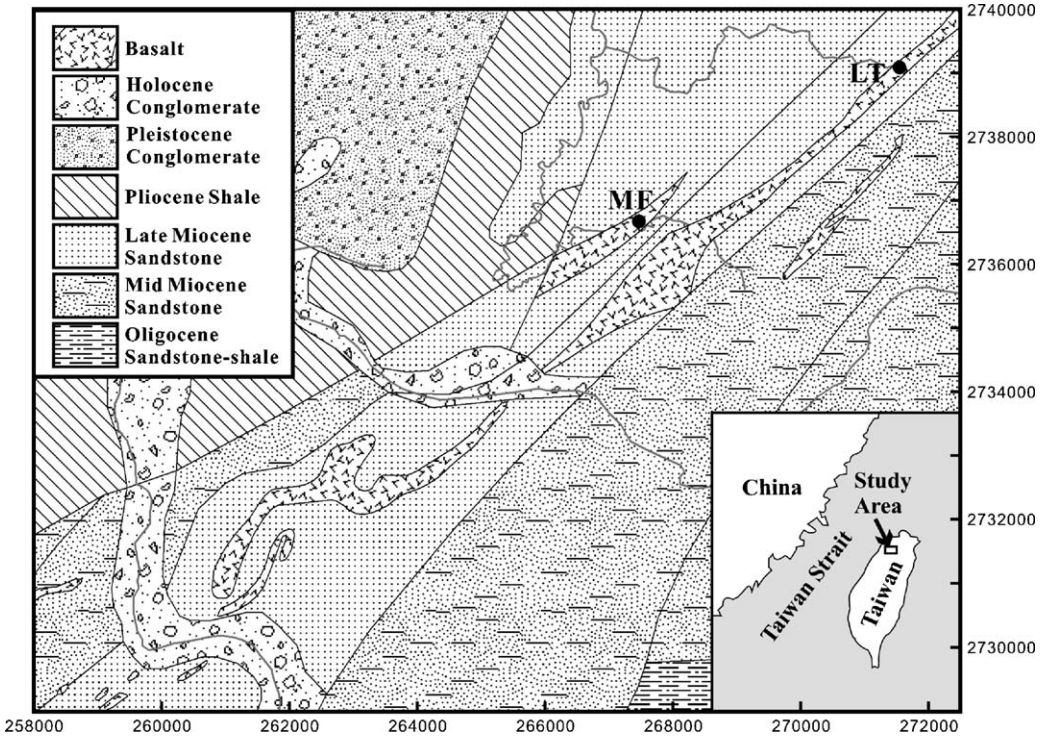

Fig. 1. Geological map of the Kuanhsi-Chutung area showing the 2 sampled localities (LT and MF).

Table 1
Stratigraphic column in the Kuanhsi-Chutung area (Tu and Chen, 1991).

Age	Lithology
Holocene	Conglomerate interbedded with mud and sand beds
Pleistocene	Lateritized conglomerate interbedded with sand beds
Pliocene	Shale interbedded with sandstone
Miocene	3rd transgressive shale sequence (the cap rock of the target CO_2 sequestration reservoir)
	3rd regressive sandstone sequence (the target CO_2 sequestration reservoir)
	2nd transgressive shale sequence
	2nd regressive sandstone sequence
	1st transgressive shale sequences
	1st regressive sandstone sequence
Oligocene	Sandstone interbedded with shale
Eocene	Sandstone interbedded with shale but there is
Paleocene	no outcrop in the study area

of CO_2 because of their great thickness and high porosity. In addition, the chemistry of the rocks and their hydrological systems can positively affect the chemical trapping CO_2 by mineral precipitation as well as effectively confine the CO_2 in a marine formation to prevent leakage. Consequently, the three Miocene terrestrial strata are considered excellent reservoirs for CO_2 sequestration. The terrestrial formation in the final Miocene depositional cycle is the target reservoir in the study area.

Miocene rifting in the China continental margin ceased at about 6.5 Ma due to a major orogeny event caused by the collision between the Eurasian Plate and the Luzon volcanic arc. Since that time the rift basin has become a foreland basin, and been subsequently filled with fine-grained marine sediments from the late Miocene to Pliocene (Table 1). This Pliocene shale is the effective confining formation for the target reservoir sandstone found in the final Miocene depositional cycle. In addition, strata in the Miocene rift basin and Pliocene foreland basin, including the CO_2 reservoir and low permeable caprock, were simultaneously deformed into an imbricate fold belt capable of hydrodynamically trapping supercritical CO_2 fluid.

2.2. Miocene basalt magmatism

As mentioned above, the Eurasian Plate Margin was under an extensional tectonic regime since the Eocene due to a decrease in convergence velocity. During this time, intraplate-type alkali basalts started to intrude into the extensional basins. There are two major basalt intrusion events in the area one during the late Oligocene and the other in the late Miocene (Chung et al., 1995a,b; Chen and Chung, 1985). The late Oligocene basalts mainly distribute in the Shuehshan Range, which is the major mountain range in central Taiwan. The Shuehshan Range was uplifted by plate collision at 3–5 Ma. Mountain heights now range between 1000 m and 2500 m. The strata in the Shuehshan Range were highly deformed which is evidenced by tight folding. Therefore, the Oligocene basalt is not suitable for CO_2 storage.

In Taiwan's Western Foothills along the westward side of the Shuehshan Range, late Miocene basalts extensively intrude into Miocene strata. The Western Foothills are hundreds of meters above sea level and the strata only mildly folded. Most of Taiwan's petroleum reservoirs are located in this region because of natural trapping structures. The Kuanhsi-Chutung area is located in the Western Foothills. The region is thought to have great potential for the sequestrating of CO_2. Late Miocene basalts also outcrop along the East Coast Mountain Range, which is orogeny resulting from the Eurasian Plate colliding with the Philippine Sea Plate. In this region, the basalt is mainly composed of basaltic glass and pillow lava from deep-sea eruptions of magma. The formations are interpreted as part of an ophiolite suite (Yui and Jeng, 1990). The CO_2 sequestration potential of the East Coast Mountain Range, however, needs further evaluation.

The thickness of late Miocene basalt in the Kuanhsi-Chutung area ranges from tens to hundreds of meters and a large amount of ultramafic xenoliths are enclosed in the basalt formation. Both the basalt and ultramafic xenoliths show carbonatization. These conditions are preferred for the chemical trapping of CO_2. In addition, the coarse-grained xenoliths are superior material for demonstrating mineral alteration and were studied as a natural analogue to CO_2 mineralization in this study.

3. Methods

3.1. Samples and analytical methods

Two types of rock samples were collected from 2 localities (LT and MF) in the Kuanhsi-Chutung area: basalts and ultramafic xenoliths (Fig. 1). These samples were firstly studied by petrographic analysis. Mineralogical assemblage was subsequently determined in detail by X-ray powder diffraction analysis (XRD). The samples for the XRD analysis were prepared by gently grinding rock samples into <10 μm powders in an agate mortar. The powders were then packed into a sample holder and analyzed by Philips powder diffractometer at the Geochemistry Laboratory of Academic Sinica, Taiwan. The results show that carbonate is the dominant phase in most samples and may overprint the signals of other minor phases. After the major mineral phases were determined, the samples were treated with hydrochloric acid to remove carbonate. The residual powders were mounted on a glass slide for determining mineral minor phases.

Electron microprobes (EMP) use a very small beam size (<3 μm) to investigate variation in chemical compositions across a single mineral grain. This variation represents geochemical evolution during crystal growth and mineral alteration. The rock sample was mounted in a 1-in. diameter epoxy disk, and then polished to give a smooth surface. Most rock samples are composed of non-conductive silicate; therefore, the sample surface must be coated with a thin film of carbon by means of evaporative deposition to dissipate accumulated electrons. The instrument used is a Shimadzu-ARL electron microprobe model EMX-SM equipped with a 4-channel wavelength-dispersive spectrometer. The acceleration potential and sample current were set at 15 kV and 10 nA, respectively. Counting times were 100 s in total (20 s for 5 replicates) on characteristic X-ray lines and backgrounds. Two beam sizes were adopted according to mineral type: <5 μm (focus electron beam) for anhydrous silicates and 15 μm (defocused electron beam) for hydrous silicates and carbonates.

X-ray fluorescence (XRF) was used to determine the bulk chemical compositions of basalts and ultramafic xenoliths. To produce a glass disk for XRF analysis, the rock sample was crushed and ground into powder of particle size <100 μm. The powder was dried at 110 °C for 24 h. Then 0.4 g of the dried powder was mixed with anhydrous lithium tetraborate ($Li_2B_4O_7$) flux in a 5% gold/95% platinum crucible and was fused into a glass disk in an automatic fusion machine. Finally, the glass disks were analyzed for ten major elements reported as oxides, including: SiO_2, TiO_2, Al_2O_3, Fe_2O_3, MnO, MgO, CaO, Na_2O, K_2O and P_2O_5, by Rigaku RIX2000 spectrometer at National Taiwan University, Taiwan.

For the analysis of the stable isotopic compositions of carbon and oxygen, the xenoliths were crushed into coarse particles and the carbonate grains were gathered with a reflected light microscope. The selected carbonate grains were crushed into fine powder and reacted with phosphate acid at 25 °C to extract CO_2 gas in a vacuum system. The CO_2 gas was then analyzed by a micromass

Table 2
Mineralogical assemblages of ultramafic xenoliths determined by XRD and EMP.

Sample	Mineralogical assemblage
LT-01	Diopside, spinel, saponite, nontronite-like mineral, calcite, ferroan dolomite, ferroan magnesite, quartz, mica
LT-02	Forsterite, enstatite, diopside, spinel, serpentine
LT-03	Forsterite, enstatite, diopside, spinel, serpentine, saponite
LT-04	Diopside, saponite, ferroan dolomite, calcite, quartz, mica
LT-05	Diopside, saponite, ferroan dolomite, calcite, quartz, mica
LT-06	Diopside, spinel, saponite, nontronite-like mineral, calcite, ferroan dolomite, ferroan magnesite, quartz, mica
LT-07	Diopside, spinel, saponite, smectite, calcite, quartz,
LT-08	Diopside, saponite, nontronite-like mineral, calcite, quartz, mica
LT-09	Diopside, spinel, saponite, nontronite-like mineral, calcite, quartz, mica
LT-10	Forsterite, enstatite, diopside, spinel, serpentine, nontronite-like mineral
LT-11	Forsterite, enstatite, diopside, spinel, nontronite-like mineral
LT-12	Forsterite, enstatite, diopside, spinel, nontronite-like mineral
LT-13	Saponite, calcite, ferroan dolomite, quartz, mica
MF-01	Saponite, calcite, ferroan dolomite, quartz, mica
MF-02	Saponite, calcite, ferroan dolomite, quartz, mica
MF-03	Forsterite, enstatite, diopside, spinel, serpentine, calcite, saponite
MF-04	Forsterite, enstatite, diopside, spinel, serpentine, saponite
MF-05	Saponite, calcite, ferroan dolomite, ferroan magnesite, quartz, mica

isotope ratio mass spectrometer at the Isotope Hydrology Laboratory of Academic Sinica, Taiwan. All isotopic ratio results are reported using the δ-notation as a per mill (‰) relative to the international Vienna Standard Mean Ocean Water (SMOW) for oxygen isotopes and to *Belemnitella americana* from the Cretaceous Pee Dee formation in South Carolina (PDB) for carbon isotopes.

4. Results and discussion

4.1. Serpentinization

In the Kuanhsi-Chutung area, carbonate veins can be extensively observed in basalt, ultramafic xenoliths and tuff, all of which demonstrates the potential to trap CO_2 in the late Miocene strata. The thickness of carbonate veins can reach 2 cm in tuff but is less than 0.5 cm in basalt. Carbonates also fill vesicles in the basalt and tuff. In general, the intensity of carbonation is simply controlled by the porosity and permeability of the rocks. According to petrographic observation, two stages of geochemical processes are recognized in basalt and its enclosed ultramafic xenoliths: (1) an earlier serpentinization stage, and (2) a later carbonate mineralization stage. The alteration sequence is evidenced by the fact that carbonate is usually associated with saponite, which is an alteration product of earlier serpentine. In this study, the mineralogical assemblages of 18 ultramafic xenoliths are mainly determined by XRD analysis. Some minerals in small amounts or in poor crystalline structure cannot be detected. Under these circumstances, EMP and petrographic analyses are conducted to complete the list of mineralogical assemblages in as much detail as possible (Table 2). It should be noted that the minerals listed in Table 2 represent only the major mineral assemblages of xenoliths and they are not in order of abundance. A procedural example of the analysis technique can be seen for LT-08 in Fig. 2. According to the database published by USGS (Chen, 1977), the results of XRD for the highly altered xenolith (LT-08) give only calcite, Mg-calcite, mica and one clay mineral with a major peak at 6.96° 2θ (Fig. 2). This clay mineral is then identified as iron-rich saponite by EMP analysis (Table 3). One difficulty is that some mineral grains have a high water content, which causes serious signal drop in EMP analysis; therefore, exact chemical compositions cannot be determined. However, because this unknown

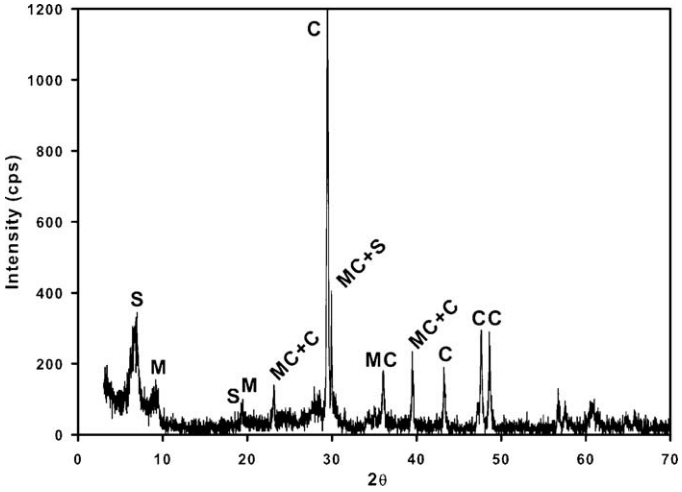

Fig. 2. XRD pattern of a highly altered xenolith (LT-08). Descriptors C, MC, M and S represent calcite, Mg-calcite, mica and saponite, respectively.

hydrous mineral is enriched with iron in EMP analysis and associated with iron-rich saponite, it may be a ferric rich member of smectite, nontronite. Nontronite can be produced by saponite oxidation; however, it is still an undetermined mineral and is named as nontronite-like mineral in this study (Mas et al., 2008). Conclusively, dolomite, magnesite, diopside and spinel can only be identified by EMP although there are suspicious peaks in some cases; the chemical variation of carbonates are also mainly determined by EMP; and calcite, saponite, mica, serpentine, forsterite and enstatite show observable signals in XRD.

The mineral assemblages of LT-11 and LT-12 demonstrate that the ultramafic xenoliths are mainly composed of forsterite, enstatite, diopside and accessory spinel. During the serpentinization processes, olivine and enstatite are readily converted into serpentine according to the simplified reaction:

$$\underset{\text{Forsterite}}{Mg_2SiO_4} + \underset{\text{Enstatite}}{MgSiO_3} + 2H_2O \rightarrow \underset{\text{Serpentine}}{Mg_3Si_2O_5(OH)_4} \quad (1)$$

Diopside and spinel are resistant to alteration as the results shown in Table 3. Spinels are generally recognized as a predominantly resistant mineral. By contrast, the stability of diopside is highly dependent on temperature, pH, and activity of Ca^{2+} in fluid (Frost and Beard, 2007); it can be a useful constraint on geochemical environments of serpentinization. In general, diopside is unstable in fluids due to tremolite-forming reactions and

Table 3
Major element analyses of selected diopside and spinel in altered ultramafic xenoliths.

Wt%	Iron-rich saponite		Diopside		Spinel	
	LT-08	MF-03	LT-01	MF-03	LT-01	MF-03
SiO_2	45.79	45.37	52.74	53.49	–	–
CaO	2.21	1.38	23.2	22.85	–	–
Na_2O	0.03	0.05	0.68	0.81	–	–
K_2O	0.01	0.03	0.01	nd	–	–
TiO_2	–	–	0.17	0.16	–	–
Al_2O_3	7.11	7.95	3.51	3.25	51.43	50.24
MgO	18.93	20.54	16.83	16.62	17.74	18.66
$\sum$FeO	13.34	10.38	1.78	1.86	9.14	9.17
MnO	0.03	0.02	0.15	0.13	0.17	0.12
Cr_2O_3	1.45	1.15	0.96	0.7	20.45	22.21
Total	88.90	86.87	100.03	99.87	98.93	100.4

nd: not detected.

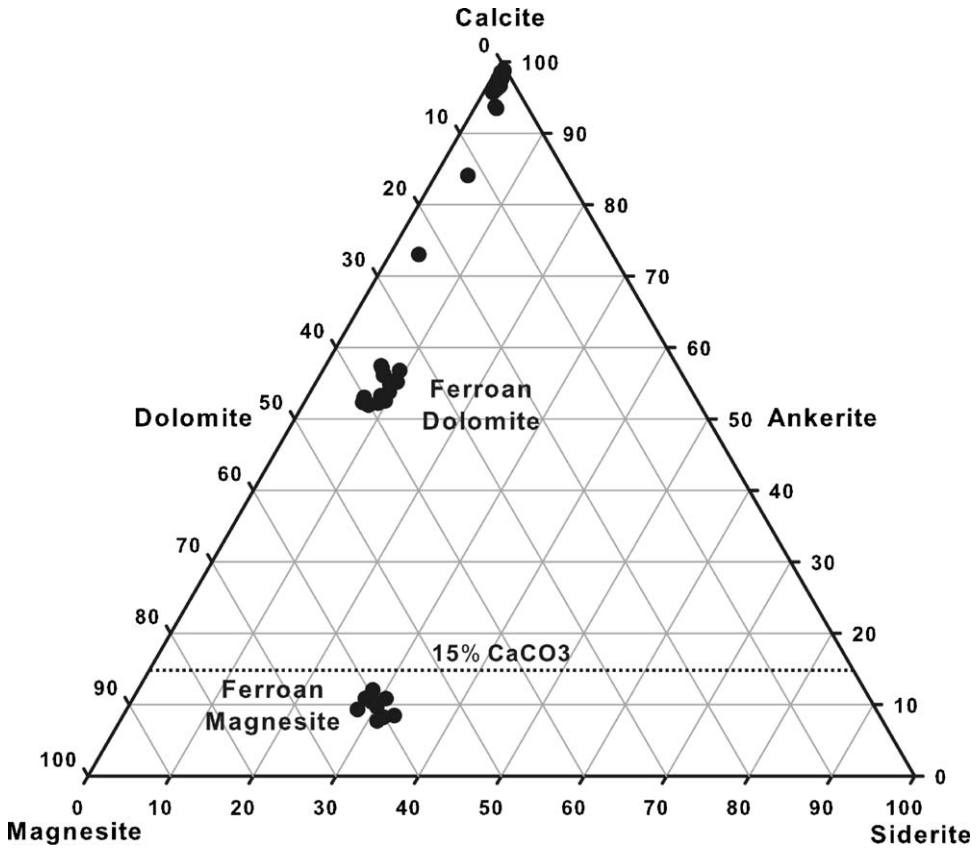

Fig. 3. Chemical compositions of selected carbonates from the basalts and ultramafic xenoliths in the Kuanhsi-Chutung area.

serpentine-forming reactions during serpentinization:

$$\underset{\text{serpentine}}{Mg_3Si_2O_5(OH)_4} + 2\underset{\text{diopside}}{CaMgSi_2O_6} + 2SiO_2 \rightarrow \underset{\text{tremolite}}{Ca_2Mg_5Si_8O_{22}(OH)_2} + H_2O \quad (2)$$

$$3\underset{\text{diopside}}{CaMgSi_2O_6} + 6H^+ \rightarrow \underset{\text{serpentine}}{Mg_3Si_2O_5(OH)_4} + 3Ca^{2+} + H_2O + 4SiO_2 \quad (3)$$

The tremolite-forming reaction (Eq. (2)) is characteristic of regional metamorphism of ultramafic rocks (Evans, 1977) and is less likely to occur in hydrothermal alteration systems as is the case in this study. Diopside, however, is readily dissolved in low-temperature environments according to the serpentine-forming reaction (Eq. (3)). Therefore, assemblages of unaltered diopside and serpentine in the case of this study are considered indicative of high concentrations of Ca^{2+} in the fluid, favoring the reverse direction of the reaction in Eq. (3).

4.2. Carbonation

The subsequent carbonation reaction in the study area is characterized by carbonates and iron-rich saponite. The carbonates include calcite, ferroan dolomite, and ferroan magnesite. The chemical compositions of selected carbonates are determined with EMP analysis as shown in Fig. 3. According to studies on carbonates precipitating under temperatures lower than 150 °C, natural/synthetic magnesite–siderite solid solutions show a considerable incorporation of $CaCO_3$ (up to 30 mol%) in the crystal structures (e.g. Romanek et al., 2009; Woods and Garrels, 1992; Königsberger et al., 1999) and higher proportions of $CaCO_3$ occur only at higher temperatures (>250 °C) (Anovitz and Essene, 1987). As shown in Fig. 3, the magnesite grains in Kuanhsi-Chutung area contain low levels of $CaCO_3$ (<15%), indicating low-temperature precipitation. The absence of high-iron carbonates, such as siderite and ankerite, demonstrates that $\log(Fe^{2+}/Ca^{2+})$ in solution is less than −3.0 (Woods and Garrels, 1992). Generally, the serpentinization of forsterite and enstatite principally releases ions of Mg^{2+} and Fe^{2+} because both minerals contain >30% of Mg^{2+} and 5–8% of Fe^{2+}.

The EMP analysis reveals geochemical variation of a selected carbonate crystal from core to rim (Fig. 4). The core is composed of pure calcite, which contains <1% of MgO and FeO. The core calcite is enclosed by ferroan dolomite; and the FeO and MgO increase

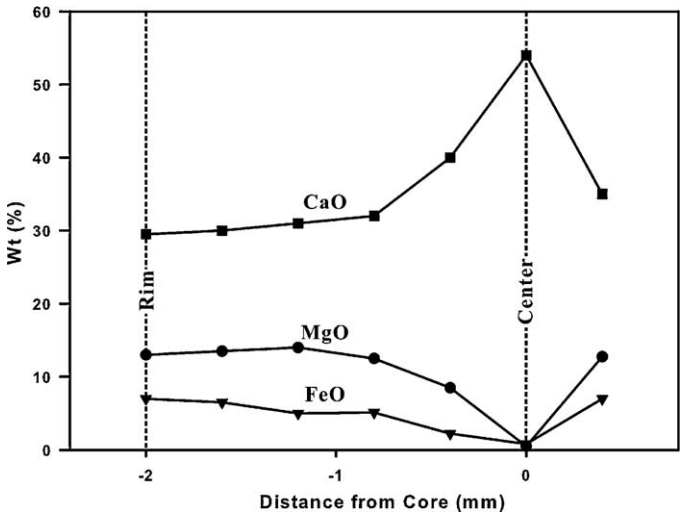

Fig. 4. Geochemical profile of a carbonate grain from core to rim.

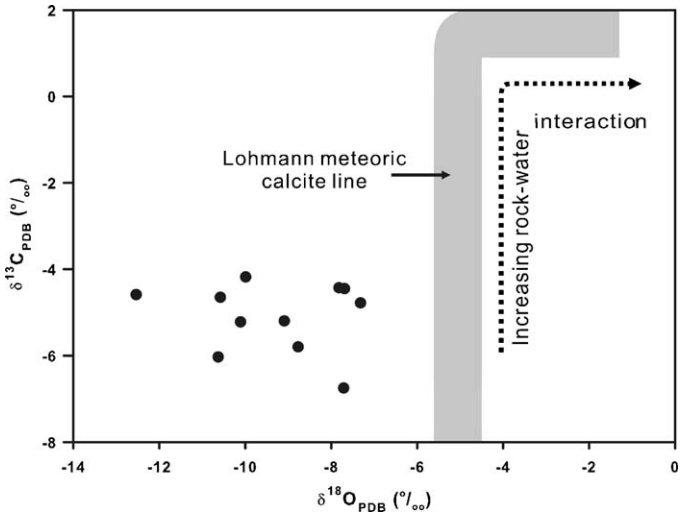

Fig. 5. Comparison between an idealized plot of variation in $\delta^{18}O$ and $\delta^{13}C$ characteristics of meteoric carbonates (Lohmann, 1988) and the isotopic compositions of carbonates from the Kuanhsi-Chutung area.

gradually from core to rim as shown in Fig. 4. The laboratory results of Golden et al. (2000) demonstrated that the geochemical composition of carbonates is more a function of the composition of the precipitating fluid than the temperature and pressure (Anovitz and Essene, 1987). Accordingly, the zoning structure of the carbonate grains in this study represents an increase in Mg^{2+} and Fe^{2+} in the fluid. In addition, Hendry (2002) suggests that the contents of Mg^{2+} and Fe^{2+} commonly show opposite behavior in carbonate directly precipitated from fluid because Fe^{2+} has a much higher partition coefficient (>1) than Mg^{2+} does (<0.05). However, Fig. 4 shows that the carbonates have covariant trends in Mg^{2+} and Fe^{2+} concentration. Therefore, the high Fe–Mg carbonates are most probably the product of the altering of core pure calcite in high Mg^{2+} and Fe^{2+} fluid due to serpentinization of mafic and ultramafic host rocks.

4.3. Isotope geochemistry

The stable isotopes ($\delta^{18}O$ and $\delta^{13}C$) of 11 carbonate samples from Kuanhsi-Chutung area were also analyzed. In order to compare with the results of other studies, the oxygen isotopic compositions referenced to the SMOW scale are converted to the PDB scale using 1.03086 for the CO_2–H_2O fractionation (Anderson and Arthur, 1983):

$$\delta^{18}O_{PDB} = 0.970\delta^{18}O_{SMOW} - 29.936 \quad (4)$$

The converted results are plotted with the Lohmann meteoric calcite line in Fig. 5. The isotopes of carbon and oxygen are predominant indicators of the fluid source and diagenetic environments during carbonation. Lohmann (1988) shows that meteoric carbonates will tend to have relatively low oxygen isotopic ratios due to the much lighter oxygen isotope of meteoric water, while marine carbonates have higher oxygen isotopic ratios. In addition, the $\delta^{13}C$ values of carbonates at shallow depth will tend to be more negative than those in the deeper zone because of more direct access of infiltrating waters to light soil CO_2 gas, which is associated with biochemical fermentation and/or thermochemical degradation of organic matter. During increased rock–water interaction, the $\delta^{13}C$ values are expected to increase and the idealized evolution in $\delta^{18}O$ and $\delta^{13}C$ is called the 'Lohmann meteoric calcite line' as shown in Fig. 5 (Anderson and Arthur, 1983; Lohmann, 1988). The carbonates measured in the study are also characterized by negative values of $\delta^{18}O$ and $\delta^{13}C$ but have lighter $\delta^{18}O$ values, ranging from −13‰ to −7‰, than would be expected from the Lohmann calcite line (Fig. 5). On the other hand, the values of $\delta^{13}C$ range from −7‰ to −4‰. This suggests that the carbonation process occurred at shallow depth; otherwise, the carbon isotope ratios would have evolved to the higher values due to profound water–rock interaction as per the trend in the Lohmann meteoric calcite line (Fig. 5).

Table 4
Potential maximum temperatures of carbonation calculated by three empirical equations assuming $\delta^{18}O_{water}$ = 0‰.

Sample	$\delta^{18}O_{calcite}$ (‰ PDB)	T (°C)[a]	T (°C)[b]	T (°C)[c]
LT-01	−10.58	74.35	77.21	73.74
LT-04	−9.99	70.33	72.69	69.81
LT-06	−12.54	88.36	93.64	87.50
LT-07	−10.63	74.70	77.60	74.08
LT-09	−10.11	71.14	73.59	70.60
LT-13	−9.09	64.37	66.12	63.98
MF-01	−7.82	56.32	57.47	56.10
MF-01	−7.71	55.65	56.75	55.43
MF-02	−7.69	55.52	56.62	55.31
MF-03	−8.77	62.31	63.88	61.96
MF-05	−7.32	53.27	54.24	53.10

The temperatures are calculated by empirical equations from: (a) Anderson and Arthur (1983), (b) Friedman and O'Neil (1977) and (c) Kim and O'Neil (1997).

Although EMP analysis identifies a few grains of high-Mg calcite (Fig. 3), which is generally related to marine origin, the oxygen isotope composition of carbonates reflects the low $\delta^{18}O$ of meteorically derived pore fluids as aforementioned (Lohmann, 1988; Hays and Grossman, 1991; Knauth et al., 2003). In addition, the results of XRD analysis show no considerable amount of dolomite or magnesite. These high-Mg carbonates should be related to the high Mg–Fe fluid caused by serpentinization process.

Temperature is the other major factor affecting oxygen stable isotope ratios and could have caused the lower oxygen isotopic composition in this study case. Urey (1947) established the oxygen isotope geothermometer based on isotope partitioning between two phases under equilibrium. For an inorganic carbonate precipitation system, there are several equations for calculating the temperature at which carbonate precipitates from water. Anderson and Arthur (1983) gave a widely used equation based on a laboratory synthetic carbonate:

$$T = 16.0 - 4.14(\delta^{18}O_{calcite} - \delta^{18}O_{water}) + 0.13(\delta^{18}O_{calcite} - \delta^{18}O_{water})^2 \quad (5)$$

where T is the temperature of calcite precipitation in °C; $\delta^{18}O_{calcite}$ is the oxygen isotope ratio in calcite relative to the PDB standard; and δ_{water} is the ratio in water relative to the SMOW standard. To use these empirical equations, the isotopic ratio of water ($\delta^{18}O_{water}$) is essential for calculating temperature of carbonation; however, it cannot be derived. As aforementioned, oxygen and carbon isotopes reveal that the water of carbonation is dominantly from a meteoric source with a negative oxygen isotope ratio. Assuming a possible maximum ratio of 0‰ for the oxygen isotope composition of water ($\delta^{18}O_{water}$ = 0‰), the potential maximum temperature of carbonation can be calculated by empirical equations (Friedman and O'Neil, 1977; Anderson and Arthur, 1983; Kim and O'Neil, 1997) as listed in Table 4. The results show inconsiderable variation in calculated temperatures (<±5 °C) using the different empirical equations. The mid-values based on Eq. (5) (Anderson and Arthur, 1983) are simply chosen to constrain the carbonation temperature in this study as shown in Fig. 6. The potential maximum temperatures of carbonation roughly range from 53 to 88 °C, which is equivalent to a depth of 1–2 km with a normal geothermal gradient (30 °C/km). This is in the preferable range for CO_2 geological sequestration. However, according to our previous analysis of meteoric water, carbonation should be taking place at shallower depth due to the assumption of a higher $\delta^{18}O_{water}$ value (0‰). Conclusively then, isotopic chem-

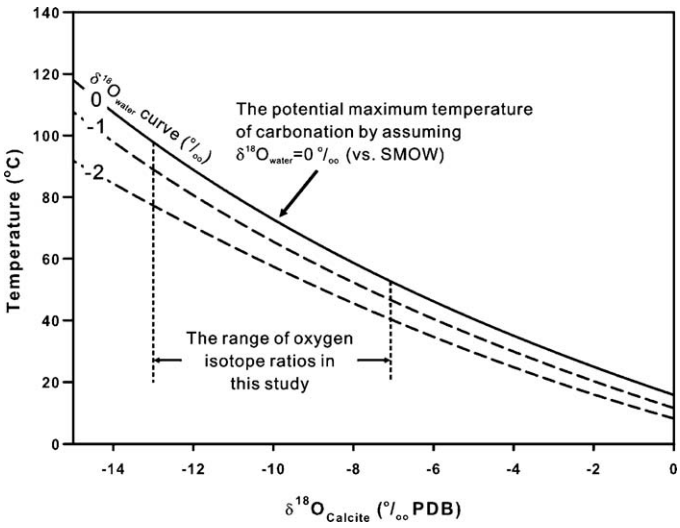

Fig. 6. Graph showing the ranges of estimated carbonation temperatures (using the equation of Friedman and O'Neil, 1977) obtained from measured $\delta^{18}O$ carbonate values and assumed $\delta^{18}O$ water values (0‰).

istry demonstrates that the carbonates in the Miocene basalt and ultramafic xenoliths precipitated under low temperature at a depth suitable for a CO_2 sequestration reservoir.

4.4. Semi-quantitative evaluation of carbonate mineralization

The results of geochemical and isotopic analyses demonstrate that the Miocene basalts and enclosed xenoliths have potential to enhance the effect of carbonate mineralization. However, it is impossible to quantitatively estimate this capacity because the composition of fluid causing carbonation cannot be precisely evaluated. Alternatively, mineral transformation from fresh xenoliths to highly altered xenoliths can be calculated for estimating the amount of carbonate precipitation. The bulk chemical compositions of three samples, including fresh xenoliths, highly altered xenoliths, and fresh basalt, are measured with XRF. The results are shown in Table 5. For conversion to normative mineralogical compositions, SINCLAS is used for calculating CIPW norms of the fresh samples (Verma et al., 2002). The advantage of SINCLAS is that the Fe_2O_3/FeO ratio can be automatically adjusted in an iterative way based on rock type and total Fe_2O_3 from XRF analysis can be properly distributed into Fe_2O_3 and FeO. There are two models that can be chosen using SINCLAS (Middlemost, 1989; Le Maitre, 1976); however, in this study, they offer limited difference (±2%) in the amounts of olivine and hypersthenes and use of either model should not cause any major difference in estimating carbonate mineralization capacity. The calculated amounts of normative minerals are listed in Table 6.

Table 5
Bulk chemistry of three igneous rock samples from the Kuanhsi-Chutung area.

	Fresh xenoliths	Fresh basalt[a]	Altered xenoliths
SiO_2	44.30	46.46	22.35
TiO_2	0.04	2.82	0.03
Al_2O_3	1.61	13.58	1.16
$\sum Fe_2O_3$	9.43	10.77	2.18
MnO	0.15	0.16	0.63
MgO	39.68	9.19	5.26
CaO	2.11	8.32	59.09
Na_2O	nd	3.48	nd
K_2O	nd	2.13	0.02
P_2O_5	0.02	0.84	0.02
Total	97.32	97.75	90.74

nd: not detected.
[a] The geochemical compositions were published in Chung et al. (1995a).

For highly altered samples, the CIPW algorithm is not suitable because alteration processes have considerable amounts of mass transfer between the mineral phase and fluid systems and the alteration products are generally hydrous minerals. Therefore, instead of the CIPW algorithm, MINSQ is used for highly altered xenoliths (Herrmann and Berry, 2002). MINSQ utilizes the Solver tool in Microsoft Excel to quantitatively estimate the proportions of constituent minerals from bulk chemical compositions. The calculation process fits the amount of presumed mineral assemblage to selected bulk chemical compositions. The fitted results are generally not unique. Thus, a result with a minimal deviation from all selected chemical compositions is desired. In this study, the mineral assemblages are determined by XRD analysis and can provide better constraints for MINSQ calculation. In addition, the primary minerals in fresh xenoliths and alteration products of serpentinization and carbonation are included in the calculation of MINSQ.

The results of normative calculations (Table 6) demonstrate findings that can be further examined to obtain a better estimation of CO_2 sequestration:

(1) Olivine and hypersthene are totally eroded away during alteration.
(2) Only small amounts of anorthite can survive, implying that the feldspar-group minerals are potentially dissolved in CO_2-rich fluid. According Kampman et al. (2009), feldspar minerals (plagioclase + orthoclase) can be altered into clay minerals with precipitation of calcite and quartz. This is consistent with the results in this study (Table 6).
(3) Diopside content increases from 4.85% to 7.23%, which is consistent with the petrographic observation that diopside is resistant to serpentinization as previously mentioned. The incremental increase in diopside is possibly caused by the replacement of heavy Fe–Mg silicates by light carbonates and hydrous minerals during alteration.
(4) Serpentine is readily replaced by carbonate during the later carbonation process; otherwise, serpentine would be much higher than 4.15% due to high forsterite and enstatite contents. Saponite, however, is more stable because it is generated from serpentine during carbonation as observed in petrographic analysis. However, the amount of saponite is minor (5.65%) in highly altered xenoliths.
(5) The Ca^{2+} contents are low in ultramafic xenoliths (2.11%) and basalt (8.32%) as shown in Table 5. Moreover, diopside is resistant to alteration and anorthite is the only mineral phase to release Ca^{2+} into fluid, which means that only half of the Ca^{2+} in ultramafic and mafic rocks is available for alteration fluid. Apparently, this amount of Ca^{2+} is not enough to cause an altered xenoliths with >59% carbonates (Table 5). Therefore, Ca^{2+} in fluid must have additional sources outside the host basalt.
(6) Calcite is the dominant carbonate and high Fe–Mg carbonates (dolomite and magnesite) are insignificant. In addition, diopside is resistant to alteration. The fluid causing alteration must be enriched with calcium; otherwise, diopside would decompose in the low temperature environment.

Conclusively, under CO_2 and Ca^{2+} enriched fluid conditions, the geochemical reactions of serpentinization and carbonation can convert all Fe–Mg silicates and most of the feldspars into calcite, quartz, small amounts of saponite and clay minerals. Bruni et al. (2002) reported that Ca-rich and high pH fluid is a mature aqueous facies due to interaction between meteoric waters and serpentinites. By using EQ3/6, the irreversible water–rock mass transfer between aqueous solution and host rock is simulated by assuming

Table 6
Normative mineralogical compositions calculated by SINCLAS and MINSQ.

Normative Minerals		Fresh xenoliths % (SINCLAS)	Altered xenoliths % (MINSQ)	Fresh basalt % (SINCLAS)
Primary minerals	Olivine	59.46	–	16.86
	Enstatite	28.85	–	–
	Diopside	4.85	7.23	17.08
	Anorthite	4.55	1.01	15.63
	Plagioclase	–	–	21.88
	Orthoclase	–	–	12.99
	Nepheline	–	–	4.61
	Ilmenite	0.08	0.03	5.53
	Magnetite	2.16	–	3.42
	Apatite	0.05	0.05	2.01
Alteration products	Serpentine	–	4.15	–
	Saponite	–	5.65	–
	Calcite	–	59.47	–
	Magnesite	–	0.00	–
	Dolomite	–	0.00	–
	Quartz	–	13.16	–
	Illite	–	0.11	–
	Kaolinite	–	0.00	–

dissolution of serpentines and precipitation of gibbsite, goethite, calcite, hydromagnesite, kaolinite, montmorillonite, saponite, sepiolite, and serpentine. The calculated hydrochemistry of the aqueous solution agrees with the analytical data. The assumed mineral assemblages to be precipitated are very similar to those found in this study. Therefore, the fluid in this study has high pH as reported by Bruni et al. (2002) and prefers to react with CO_2 into carbonates.

Accordingly, the following reactions are considered as the simplified model for semi-quantitatively estimating the amount of CO_2 sequestration (Gaus et al., 2005; Lagneau et al., 2005; Worden and Barclay, 2000; Baines and Worden, 2001).

$$\underset{\text{albite}}{2NaAlSi_3O_8} + CO_2 + 2H_2O + Ca^{2+} \rightarrow \underset{\text{calcite}}{CaCO_3} + SiO_2 + \underset{\text{kaolinite}}{Al_2Si_2O_5(OH)_4} + 2Na^+ \quad (6)$$

$$\underset{\text{anorthite}}{CaAl_2Si_2O_8} + 2H_2O + CO_2 \rightarrow \underset{\text{calcite}}{CaCO_3} + \underset{\text{kaolinite}}{Al_2Si_2O_5(OH)_4} \quad (7)$$

$$\underset{\text{K-feldspar}}{3KAlSi_3O_8} + CO_2 + 2H_2O + Ca^{2+} \rightarrow \underset{\text{Illite}}{KAl_3Si_3O_{10}(OH)_4} + \underset{\text{calcite}}{CaCO_3} + \underset{\text{quartz}}{6SiO_2} + 2K^+ \quad (8)$$

$$\underset{\text{nepheline}}{2(Na, K)AlSiO_4} + CO_2 + 2H_2O + Ca^{2+} \rightarrow \underset{\text{kaolinite}}{Al_2Si_2O_5(OH)_4} + \underset{\text{calcite}}{CaCO_3} + 2(Na, K)^+ \quad (9)$$

$$\underset{\text{forsterite}}{Mg_2SiO_4} + 2CO_2 + 2Ca^{2+} \rightarrow \underset{\text{calcite}}{2CaCO_3} + 2Mg^{2+} + \underset{\text{quartz}}{SiO_2} \quad (10)$$

$$\underset{\text{enstatite}}{MgSiO_3} + CO_2 + Ca^{2+} \rightarrow \underset{\text{calcite}}{CaCO_3} + Mg^{2+} + \underset{\text{quartz}}{SiO_2} \quad (11)$$

Stoichiometric ratios of generated calcite to primary minerals in these reactions are used for calculating the amount of CO_2 potentially trapped. Two assumptions are also needed for the calculation:

(1) Basalt density is designated at 2890 kg/m^3 for converting wt% to vol%.
(2) Typical basalt porosity ranges from 15% to 20%, which is the space filled with fluid. Accordingly, the degree of carbonation of basalt is estimated to be 20%.

The calculation and results are listed in Table 7. The amount of trapped CO_2 in the Miocene basalt in Kuanhsi-Chutung area is semi-quantitatively estimated as 32.58 g/kg of basalt, which is equivalent to 94.15 kg CO_2 chemically trapped by 1 m^3 basalt. With this value, the total amount of CO_2 sequestration can be evaluated if the dimensions of the Miocene basalt in the potential sites can be revealed by geophysical investigation in the near future.

5. Conclusion

This study examines the late Miocene sandstone and enclosed basalts of the Kuanhsi-Chutung area as potential sites for CO_2 mineral sequestration. This particular region has the potential to act as a natural analogue for CO_2 sequestration. The study examines CO_2 mineral sequestration processes and analyzes CO_2 storage capac-

Table 7
Estimation of the amount of CO_2 sequestration based on the normative mineralogical composition of the Miocene basalt from the Kuanhsi-Chutung area.

Normative Minerals	Mol. ratio[a]	Wt%	Mol. (g/kg of basalt)	Max. potential trapped CO_2 (g/kg of basalt)[b]	Estimated trapped CO_2 (g/kg of basalt)[c]
Forsterite	2.00	16.86	1.20	105.98	21.20
Anorthite	1.00	15.63	0.56	24.74	4.95
Albite	0.50	21.88	0.84	18.37	3.67
K-feldspar	0.33	12.99	0.47	6.85	1.37
Nepheline	0.50	4.61	0.32	6.95	1.39
Total				162.89	32.58

[a] The Mol. ratios are determined by the carbonation reactions (Eq. (6)–(11)).
[b] The maximum potential trapped CO_2 is calculated based on 100% carbonation.
[c] The amount of trapped CO_2 is estimated with 20% carbonation.

ity. The $\delta^{13}C_{PDB}$ value of carbonates ranges from −7‰ to −4‰ indicating that carbonation process is mainly controlled by carbonate precipitation rather than water–rock interaction. In addition, oxygen stable isotopes are used to determine the temperature of carbonate precipitation. The potential maximum temperature of carbonation derived from the empirical equations ranges from 53 to 88 °C, which is equivalent to a depth of 1–2 km or shallower. This demonstrates that the carbonation process can take place at an acceptable depth for the creation of a practical CO_2 sequestration reservoir. The mineralogical assemblages of highly altered xenoliths show that diopside is resistant and all other major minerals, including forsterite, enstatite and feldspars, are readily replaced by carbonates. Based on the observed mineral transformation of xenoliths, simplified geochemical reactions of carbonation can be established and applied to evaluating the capacity for CO_2 mineral sequestration in the Miocene basalt. Using this semi-quantitative model, the Miocene basalt could sequester 94.15 kg of CO_2 per 1 m^3 basalt. The full CO_2 mineral sequestration capacity requires a geophysical survey to determine the dimensions of basalt at the site.

Acknowledgements

Special thanks to reviewers for giving constructive comments and improving our manuscript. This work was financially supported by the Bureau of Energy, Ministry of Economic Affairs, Taiwan.

References

Allen, D.E., Strazisar, B.R., Soong, Y., Hedges, S.W., 2005. Modeling carbon dioxide sequestration in saline aquifers: significance of elevated pressures and salinities. Fuel Processing Technology 86, 1569–1580.

Anderson, T.F., Arthur, M.A., 1983. Stable isotopes of oxygen and carbon and their application to sedimentologic and paleoenvironmental problems. In: Arthur, M.A., Anderson, T.F., Kaplan, I.R., Veizer, J., Land, L.S. (Eds.), Stable Isotopes in Sedimentary Geology: SEPM Short Course, vol. 10. , pp. 1–151.

Anovitz, L.M., Essene, E.J., 1987. Phase equilibria in the system $CaCO_3$–$MgCO_3$–$FeCO_3$. Journal of Petrology 28, 3S9–414.

Audigane, P., Gaus, I., Czernichowski-Lauriol, I., Pruess, K., Xu, T., 2007. Two-dimensional reactive transport modeling of CO_2 injection in a saline aquifer at the Sleipner site, North Sea. American Journal of Science 307, 974–1008.

Bachu, S., Gunter, W.D., Perkins, E.H., 1994. Aquifer disposal of CO_2: hydrodynamic and mineral trapping. Energy Conversion and Management 35, 269–279.

Bruni, J., Canepa, M., Chiodini, G., Cioni, R., Cipolli, F., Longinelli, A., Marini, L., Ottonello, G., Zuccolini, M.V., 2002. Irreversible water–rock mass transfer accompanying the generation of the neutral, Mg–HCO_3 and high-pH, Ca–OH spring waters of the Genova Province, Italy. Applied Geochemistry 17, 455–474.

Baines, S.J., Worden, R.H., 2001. Geological CO_2 disposal: understanding the long term fate of CO_2 in naturally occurring accumulations. In: Williams, D.J., McMullan, D.P., Paulson, C.A.J., Smith, A.Y. (Eds.), Greenhouse Gas Control Technologies. , pp. 311–316.

Chen, C.-H., Chung, S.L., 1985. Petrology and geochemistry of Neogene basalts and related rocks in northern Taiwan: (1) basanitoids, alkali olivine basalts and tholeiites from Kuanhsi-Chutung area. Acta Geologica Taiwanica 23, 35–62.

Chen, P.Y., 1977. Table of key lines in X-ray powder diffraction patterns of minerals in clays and associated rocks. U.S. Geological Survey Occasional Paper 21, 17–19.

Chung, S.L., Jahn, B.M., Chen, S.J., Lee, T., Chen, C.-H., 1995 a. Miocene basalts in northwestern Taiwan: evidence for EM-type mantle sources in the continental lithosphere. Geochimica et Cosmochimica Acta 59, 549–555.

Chung, S.L., Yang, T.F., Lee, C.Y., Chen, C.-H., 1995 b. The igneous provinciality in Taiwan: consequence of continental rifting superimposed by Luzon and Ryukyu subduction systems. Journal of Southeast Asian Earth Sciences 11, 73–80.

Cipolli, F., Gambardella, B., Marini, L., Ottonello, G., Zuccolini, M.V., 2003. Geochemistry of high-pH waters from serpentinites of the Gruppo di Voltri (Genova, Italy) and reaction path modeling of CO_2 sequestration in serpentinite aquifers. Applied Geochemistry 19, 787–802.

Evans, B.W., 1977. Metamorphism of alpine peridotite and serpentinite. Annual Review of Earth and Planetary Sciences 5, 398–447.

Flaathen, T.K., Gislason, S.R., Oelkers, E.H., Sveinbjörnsdóttir, A.E., 2009. Chemical evolution of the Mt. Hekla, Iceland, groundwaters: a natural analogue for CO_2 sequestration in basaltic rocks. Applied Geochemistry 24, 463–474.

Frost, B.R., Beard, J.S., 2007. On silica activity and serpentinization. Journal of Petrology 48, 1351–1368.

Friedman, I., O'Neil, J.R., 1977, Compilation of stable isotope fractionation factors of geochemical interest. U.S. Geological Survey Professional Paper 440-KK, pp. 1–12.

Gaus, I., Azaroual, M., Czernichowski-Lauriol, I., 2005. Reactive transport modelling of the impact of CO_2 injection on the clayey cap rock at Sleipner (North Sea). Chemical Geology 217, 319–337.

Gislason, S.R., Wolff-Boenisch, D., Stefansson, A., Oelkers, E.H., Gunnlaugsson, E., Sigurdardottir, H., Sigfusson, B., Broecker, W.S., Matter, J.M., Stute, M., Axelsson, G., Fridriksson, T., 2010. Mineral sequestration of carbon dioxide in basalt: a pre-injection overview of the CarbFix project. International Journal of Greenhouse Gas Control 4, 537–545.

Giammar, D.E., Bruant Jr., R.G., Peters, C.A., 2005. Forsterite dissolution and magnesite precipitation at conditions relevant for deep saline aquifer storage and sequestration of carbon dioxide. Chemical Geology 217, 257–276.

Gianelli, G., Grassi, S., 2001. Water–rock interaction in the active geothermal system of Pantelleria, Italy. Chemical Geology 181, 113–130.

Goel, M., Charan, S.N., Bhandari, A.K., 2009. CO_2 sequestration: recent Indian research. Glimpses of Geoscience Research in India, 56–60.

Golden, D.C., Ming, D.W., Schwandt, C.S., Morris, R.V., Yang, S.V., Lofgren, G.E., 2000. An experimental study on kinetically-driven precipitation of calcium–magnesium–iron carbonates from solution: implications for the low-temperature formation of carbonates in Martian meteorite Allan Hills 84001. Meteoritics and Planetary Science 35, 457–465.

Golubev, S.V, Pokrovsky, O.S., Schott, J., 2005. Experimental determination of the effect of dissolved CO_2 on the dissolution kinetics of Mg and Ca silicates at 25 °C. Chemical Geology 217, 227–238.

Gunter, W.D., Wiwchar, B., Perkins, E.H., 1997. Aquifer disposal of CO_2-rich greenhouse gases: extension of the time scale of experiment for CO_2-sequestering reactions by geochemical modeling. Mineralogy and Petrology 59, 121–140.

Gysi, A.P, Stefánsson, A., 2008. Numerical modelling of CO_2–water–basalt interaction. Mineralogical Magazine 72, 55–59.

Hays, P.D., Grossman, E.L., 1991. Oxygen isotopes in meteoric calcite cements as indicators of continental paleoclimate. Geology 19, 441–444.

Hendry, J.P., 2002. Geochemical trends and palaeohydrological significance of shallow burial calcite and ankerite cements in Middle Jurassic strata on the East Midlands Shelf (onshore UK). Sedimentary Geology 151, 149–176.

Herrmann, W., Berry, R.F., 2002. MINSQ; a least squares spreadsheet method for calculating mineral proportions from whole rock major element analyses. Geochemistry – Exploration, Environment, Analysis 2, 361–368.

IPCC, 2002, IPCC Workshop on Carbon Dioxide Capture and Storage, pp. 1–175.

IPCC, 2005. Carbon Dioxide Capture and Storage. IPCC Special Report. Cambridge University Press, New York, pp. 1–431.

Kampman, N., Bickle, M., Becker, J., Assayag, N., Chapman, H., 2009. Feldspar dissolution kinetics and Gibbs free energy dependence in a CO_2-enriched groundwater system, Green River, Utah. Earth and Planetary Science Letters 284, 473–488.

Kaszuba, J.P., Janecky, D.R., Snow, M.G., 2003. Carbon dioxide reaction processes in a model brine aquifer at 200 °C and 200 bars: implications for geologic sequestration of carbon. Applied Geochemistry 18, 1065–1080.

Kim, S.T., O'Neil, J.R., 1997. Equilibrium and nonequilibrium oxygen isotope effects in synthetic carbonates. Geochimica et Cosmochimica Acta 61, 3461–3475.

Knauth, L.P., Brilli, M., Klonowski, S., 2003. Isotope geochemistry of caliche developed on basalt. Geochimica et Cosmochimica Acta 67, 185–195.

Königsberger, E., Königsberger, L.-C., Gamsjäger, H., 1999. Low-temperature thermodynamic model for the system Na_2CO_3–$MgCO_3$–$CaCO_3$–H_2O. Geochimica et Cosmochimica Acta 63, 3105–3119.

Lagneau, V., Pipart, A., Catalette, H., 2005. Reactive Transport Modelling of CO_2 Sequestration in Deep Saline Aquifers. Oil and Gas Science and Technology – Revue IFP 60, 231–247.

Le Maitre, R.W., 1976. Some problems of the projection of chemical data into mineralogical classifications. Contributions of Mineralogy and Petrology 56, 181–189.

Lin, A.T., Watts, A.B., 2002. Origin of the West Taiwan basin by orogenic loading and flexure of a rifted continental margin. Journal of Geophysical Research 107 (B9), 2185.

Lohmann, K.C., 1988. Geochemical patterns of meteoric diagenetic systems and their application to studies ofpaleokarst. In: James, N.P., Choquette, P.W. (Eds.), Paleokarst. Springer-Verlagmew, New York, pp. 58–80.

Mas, A., Meunier, A., Beaufort, D., Patrier, P., Dudoignon, P., 2008. Clay minerals in basalt-hawaiite rocks from Mururoa Atoll (French Polynesia). I. Mineralogy. Clays and Clay Minerals 56, 711–729.

Matter, J.M., Broecker, W.S., Stute, M., Gislason, S.R., Oelkers, E.H., Stefánsson, A., Wolff-Boenisch, D., Gunnlaugsson, E., Axelsson, G., Björnsson, G., 2009. Permanent carbon dioxide storage into basalt: the CarbFix Pilot Project, Iceland. Energy Procedia 1, 3641–3646.

McGrail, B.P., Schaef, H.T., Ho, A.M., Chien, Y.J., Dooley, J.J., Davidson, C.L., 2006. Potential for carbon dioxide sequestration in flood basalts. Journal of Geophysical Research 111, B12201.

Middlemost, E.A.K., 1989. Iron oxidation ratios, norms and the classification of volcanic rocks. Chemical Geology 77, 19–26.

Prasad, P.S.R., Srinivasa Sarma, D., Sudhakar, L., Basavaraju, U., Singh, R.S., Begum, Z., Archana, K.B., Chavan, C.D., Charan, S.N., 2009. Geological sequestration of carbon dioxide in Deccan basalts: preliminary laboratory study. Current Science 96, 228–291.

Romanek, C.S., Jiménez-López, C., Navarro, A.R., Sánchez-Román, M., Sahai, N., Coleman, M., 2009. Inorganic synthesis of Fe–Ca–Mg carbonates at low temperature. Geochimica et Cosmochimica Acta 73, 5361–5376.

Schaef, H.T., McGrail, B.P., Owen, A.T., 2010. Carbonate mineralization of volcanic province basalts. International Journal of Greenhouse Gas Control 4, 249–261.

Soong, Y., Goodman, A.L., McCarthy-Jones, J.R., Baltrus, J.P., 2004. Experimental and simulation studies on mineral trapping of CO_2 with brine. Energy Conversion and Management 45, 1845–1859.

Tu, M.K., Chen, W.C., 1991. Explanatory text of the geologic map of Taiwan Scale 1:50000 Sheet 13 Chutung. Central Geological Survey, 1–75 (in Chinese).

Urey, H.C., 1947. The thermodynamic properties of isotopic substances. Journal of the Chemical Society, 578–579.

Verma, S.P., Torres-Alvarado, I.S., Sotelo-Rodríguez, Z.T., 2002. SINCLAS: standard igneous norm and volcanic rock classification system. Computers and Geosciences 28, 711–715.

Viete, D.R, Ranjith, P.G., 2007. The mechanical behaviour of coal with respect to CO_2 sequestration in deep coal seams. Fuel 86, 2667–2671.

Wigand, M., Carey, J.W., Schütt, H., Spangenberg, E., Erzinger, J., 2008. Geochemical effects of CO_2 sequestration in sandstones under simulated in situ conditions of deep saline aquifers. Applied Geochemistry 23, 2735–2745.

Woods, T.L., Garrels, R.M., 1992. Calculated aqueous-solution–solid-solution relations in the low-temperature system CaO–MgO–FeO–CO_2–H_2O. Geochimica et Cosmochimica Acta 56, 3031–3043.

Worden, R.H., Barclay, S.A., 2000. Internally-sourced quartz cement due to externally-derived CO_2 in sub-arkosic sandstones, North Sea. Journal of Geochemical Exploration 69–70, 645–649.

Xu, T., Apps, J.A., Pruess, K., 2004. Numerical simulation of CO_2 disposal by mineral trapping in deep aquifers. Applied Geochemistry 19, 917–936.

Yui, T.F., Jeng, R.C., 1990. A stable-isotope study of the hydrothermal alteration of the East Taiwan Ophiolite. Chemical Geology 89, 65–85.

Zerai, B., Saylor, B.Z., Matisoff, G., 2006. Computer simulation of CO_2 trapped through mineral precipitation in the Rose Run Sandstone, Ohio. Applied Geochemistry 21, 223–240.